Quantum Kicked Rotor Systems

Aditya Chincholi

June 19, 2021

Abstract

We discuss kicked rotor systems and the properties of dynamical localisation in these systems, particularly their robustness to noise. We also discuss the quasiperiodic kicked rotor and the change in its properties as it crosses the critical point of the metal-insulator transition, particularly the change in the spectrum. We present results on the evaluation of the bipartite entanglement entropy in the 3d quasiperiodic kicked rotor system.

Contents

Chapter 1

Introduction

The quantum kicked rotor is defined by the Hamiltonian:

$$H = \frac{p^2}{2} + kcos(\theta)\sum_{n\in\mathbb{Z}}\delta(t - n\tau) \tag{1.1}$$

This classical analogue of this system reduces to the Chirikov standard map [6]:

$$p_{n+1} = p_n + ksin(\theta_n) \tag{1.2}$$
$$\theta_{n+1} = \theta_n + p_{n+1} \tag{1.3}$$

This map is chaotic and shows a great deal of complexity, but we will only deal with the quantum version here. The key point for us, is that this classical map displays diffusion in the angular momentum space. This can be seen qualitatively by looking at 1.3. When p_n becomes larger than 2π, which will happen after a few kicks if k is large, then the successive θ_n will become uncorrelated. As the sign of $sin(\theta_n)$ becomes random, the sequence p_n describes a random walk. This can be backed by a quantitative calculation which shows that the distribution $f_N(p)$, i.e. the distribution of momentum after N steps wrt different initial conditions (θ_0), is well approximated by a gaussian distribution with a diffusion constant [6]:

$$D = \frac{k^2}{2} \tag{1.4}$$

As a time dependent problem, the quantum kicked rotor has no energy eigenstates. However, since it is a periodic kicking potential, we can use floquet operators to simulate it.

$$F = \lim_{\epsilon\to 0}\int_0^{\tau+\epsilon} exp(-iHt/\hbar)dt \tag{1.5}$$
$$= exp\left(\frac{-i}{\hbar}cos\ \theta\right) exp\left(\frac{-i\tau}{2\hbar}p^2\right) \tag{1.6}$$

The floquet operator allows us to obtain the state of the system at $t = n\tau$. Working in the eigenbasis of the (angular) momentum operator $p\,|n\rangle = \hbar n\,|n\rangle\,; \langle\theta|n\rangle = e^{in\theta}$, we get:

$$\langle m|F|n\rangle = exp\left(-\frac{i\tau}{2\hbar}m^2\right) i^{n-m} J_{n-m}\left(\frac{k}{\hbar}\right) \tag{1.7}$$

We can use this expression for the floquet matrix to simulate the quantum kicked rotor system as $F^N\,|\psi(0)\rangle = |\psi(N\tau)\rangle$. Even though the system doesn't have stationary states, we can obtain floquet eigenstates by diagonalising the floquet operator.

An important variant of the kicked rotor system is the quasiperiodic kicked rotor, which is discussed further in the report. It is given by the Hamiltonian:

$$H = \frac{p^2}{2} + \mathcal{K}(t)cos(\theta)\sum_{n\in\mathbb{Z}}\delta(t - n\tau) \tag{1.8}$$

where $\mathcal{K}(t) = k(1 + \epsilon cos(\omega_2 t + \phi_2)cos(\omega_3 t + \phi_3))$.

Chapter 2

Readings and Work Done

2.1 Localisation

The quantum kicked rotor also shows the same diffusion mechanism as the classical analogue in the beginning. If we take the initial state as $|0\rangle$ which has a uniform distribution of $\theta' s$, then the system shows a gaussian shape in the momentum space. But after a certain time, the diffusion is suppressed by quantum effects which lead to an exponential localisation in the momentum space distribution around $|0\rangle$. This phenomenon is called 'dynamical localisation'. It is analogueous to the Anderson localisation found in tight-binding systems.

We now simulate the system using $|\psi(N\tau)\rangle = F^N |0\rangle$. The results are shown in Figure 2.1. The figure shows the state of the system as after different number of timesteps. The initial stages ($t = 100$) show the classically expected gaussian profile in the momentum space probability distribution. But after that the quantum effects begin to dominate and we obtain a exponentially linear profile i.e. $P(p) \sim e^{-p/p_{loc}}$.

Though it is hard to see on the log scale, $\langle p^2 \rangle$ shows a lineary increasing profile during the diffusion phase (this is the same as the classical case) but then saturates as localisation occurs at longer time scales.

So why does localisation occur? Qualitatively speaking, after certain number of timesteps we see destructive interference happening for the transition amplitudes (i.e. the probability of $|m\rangle = F|n\rangle$) when we calculate the expectation $\langle p^2 \rangle$. For a more quantitative argument, the reader is encouraged to see section 4.2.1 of [6].

A different way to see the emergence of localisation is through a nonlinear transformation that connects the kicked rotor system with the Anderson model. The next section will cover the Anderson model in more detail. Here we just briefly outline the mapping, for more details see [6]. Consider a 1d quantum kicked rotor of the form:

$$H = K(p) + V(\theta) \sum_n \delta(t - n) \tag{2.1}$$

Then we obtain the floquet operator:

$$F = e^{-iV(\theta)} e^{-iK(p)} \tag{2.2}$$

$$F_{nm} = e^{-iK(m)} J_{n-m} \tag{2.3}$$

$$\text{where } J_n = \frac{1}{2\pi} \int_0^{2\pi} e^{-iV(\theta)} e^{in\theta} d\theta \tag{2.4}$$

We consider the eigenvector $\mathbf{a}$ of F with eigenphase ϕ and use the mapping $W(\theta) = -tan(V(\theta)/2)$ and $\bar{\mathbf{a}} = (e^{i(\phi - K)} + 1)\mathbf{a}$. Then we obtain:

$$tan\left(\frac{\phi - K}{2}\right) \bar{\mathbf{a}} + W \bar{\mathbf{a}} = 0 \tag{2.5}$$

Taking a fourier transform of all the components wrt θ

$$\sum_{k \neq n} W_{n-k} \bar{a_k} + E_n^0 \bar{a_n} = E \bar{a_n} \tag{2.6}$$

where $E_n^0 = tan((\phi - K(n))/2)$ and $E = -W_0$. This is the Anderson tight-binding model with bond strengths given by the W_{n-m}'s and site energies given by E_n^0's.

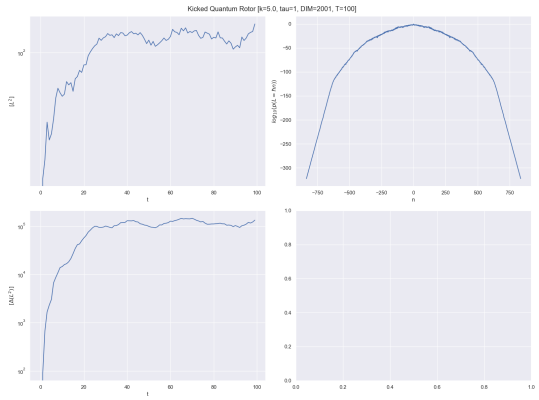

(a) After 100 timesteps.

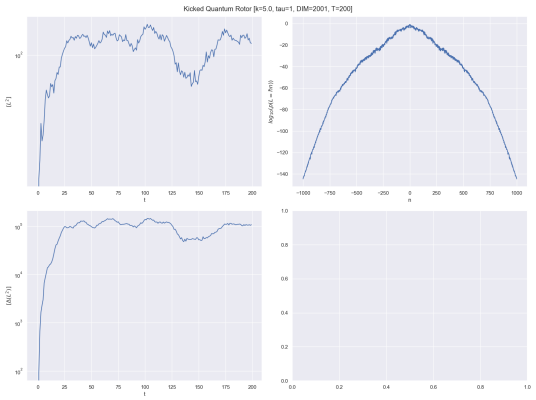

(b) After 200 timesteps

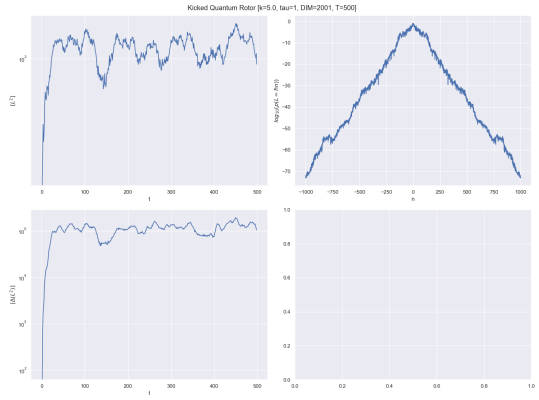

(c) After 500 timesteps.

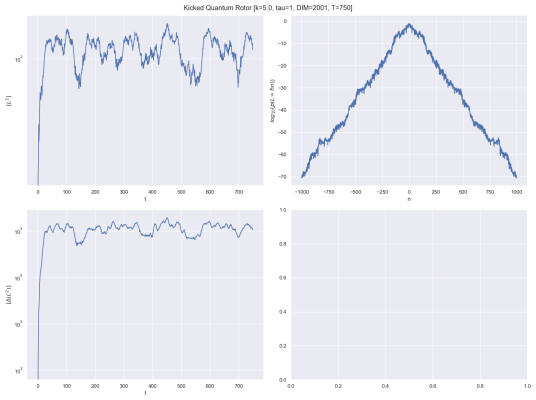

(d) After 750 timesteps.

Figure 2.1: Evolution of the kicked rotor system with $k = 5$, $\hbar = 1$ and $\tau = 1$ in a basis of $\{|-1000\rangle, ..., |1000\rangle\}$. The top left plot is $[p^2]$ vs t; top right is $log_{10}(P(p = n\hbar))$ vs n i.e the log of the probability distribution in momentum space and the bottom left plot is the variance of momentum square $[(\Delta(p^2))^2]$ vs time t.

(a) Base case with no noise.

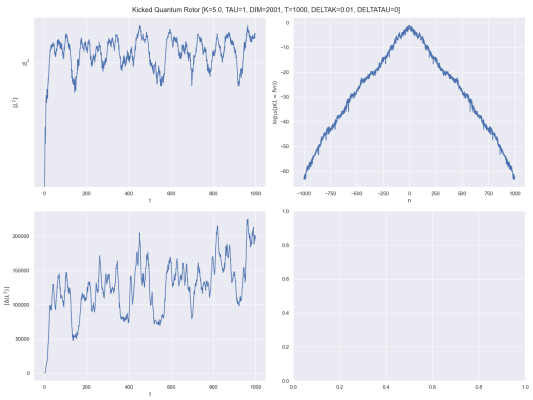

(b) $\delta k = 0.01 (0.2\ \%)$

(c) $\delta k = 0.1\ (2\ \%)$

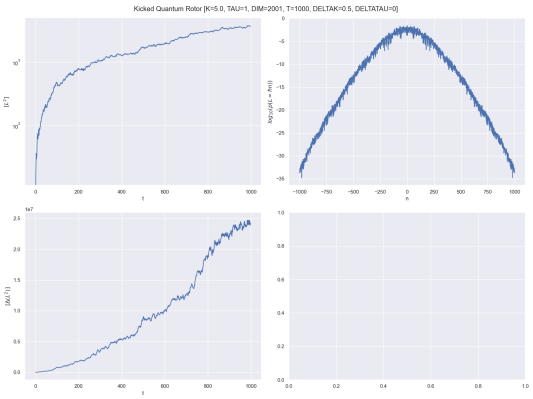

(d) $\delta k = 0.5\ (10\ \%)$

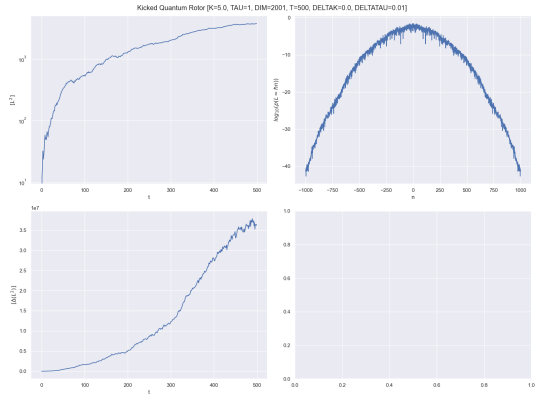

(e) $\delta \tau = 0.01\ (1\ \%)$

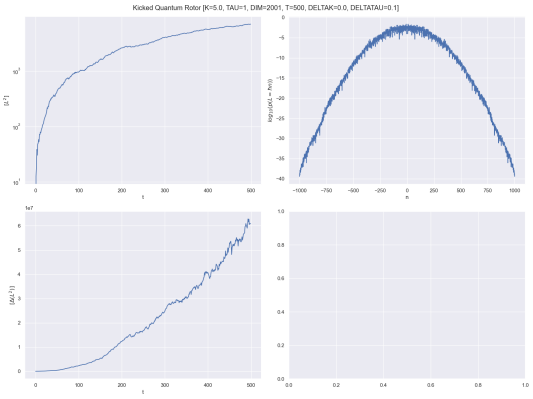

(f) $\delta \tau = 0.1\ (10\ \%)$

Figure 2.2: Evolution of the quantum kicked rotor system with a perturbative noise added to either k or τ at each stage. All runs have the base values $k = 5$, $\tau = 1$, $\hbar = 1$ and are run for either 1000 timesteps or 500 timesteps on a basis of states $\{|-1000\rangle, ... |1000\rangle\}$. Top left is average sq. momentum $[p^2]$, bottom left is variance of sq. momentum $[(\Delta(p^2))^2]$ and top right is the momentum distribution $log_{10}(P(p = n\hbar))$ vs n

2.2 Anderson Localisation

We now take a short detour to explain the phenomenon of Anderson Localisation. The contents of this section are largely taken from [5].

Consider a non-relativistic particle or gaussian wave packet propogating through a channel. If the channel has a constant potential throughtout then the wave will propogate through it unimpeded performing ballistic motion. If the channel has a constant potential with a small noise term, then the potential landscape will look like a series of speckles on an otherwise flat surface. Let us assume these speckles are well separated and look more like spikes rather than shallow hills.

We have three length scales here, l the spacing between these speckles, δ the width of the speckle and λ the de Broglie wavelength of the particle. We assume $\delta << \lambda << l$ and thus, the particle sees the speckles as well-separated δ-spikes.

Each of these speckles - wells and peaks - acts as a scatter for our particle. Quantum mechanically, each of them has a finite, non-zero probability of both reflecting and transmitting the particle.

Suppose then that our particle hits scatterer 1 and gets transmitted with some probability. It then performs ballistic motion and hits scatterer 2. Again there is some probability of transmission and reflection. The particle may get transmitted immediately, or it may undergo reflection twice (a complete internal reflection) and then get transmitted. It may undergo a complete internal reflection multiple times before crossing the scatterer. This leads to the net transmission probability being dependent on the phase difference accumulated over a complete internal reflection.

The net transmission probability can be found by multiplying the transfer matrices of the two scatterers and obtaining an overall transfer matrix. This yields the expression:

$$T_{12} = \frac{T_1 T_2}{1 + \sqrt{R_1 R_2} e^{i\theta}} \tag{2.7}$$

where T_i and R_i denote the transmission and reflection probabilities of the ith scatterer, θ is the phase accumulated in a complete internal reflection.

This phase is distributed randomly irrespective of the distribution of distances between the scatterers as $\lambda << l$ and thus, we may assume a uniform distribution for θ.

Decoherence can occur if during the ballistic part, the particle couples to an external degree of freedom. In such a scenario, we can assume a uniform distribution for θ and obtain an average transmission probability. In doing this, we are effectively killing any interference effects as we are considering the phase to be completely scrambled by the time it reaches scatterer 2. The calculations then yield $\langle T_{12} \rangle = T_1 T_2 / (1 - R_1 R_2)$. For a channel of length L and nearly uniform scatterer density n, this gives us $R/T \propto nL$ which is Ohm's law.

But things are much more interesting if we have phase-coherent transmission through the channel. We must then find a quantity that is additive for such a transmission and average over it. $\kappa = -ln\ T$ is such a quantity. It exhibits the property $\langle ln\ T_{12} \rangle = ln\ T_1 + ln\ T_2$ and due to this, it displays self-averaging.

Therefore, for a channel of length L, $|\langle ln\ T \rangle| \propto nL$. Since $T < 1$, $ln\ T < 0$ and thus we have $exp(\langle ln\ T \rangle) \sim exp(-L/\xi_{loc})$ where ξ_{loc} is called the localisation length. This exponential localisation in the absence of absorption is a hallmark of strong localisation.

Here, $ln\ T$ exhibits a normal distribution and its peak corresponds to the most likely value $T_{typ} = exp(\langle ln\ T \rangle) = e^{-L/\xi_{loc}}$. This phenomenon is called Anderson localisation.

In 3D, the situation becomes more complicated and the system can either allow transmission or show localisation based on disorder strength. These two regimes are separated by a 2nd order phase transition known as the Anderson transition or the metal-insulator transition, metal referring to transmission and insulator referring to localisation of the particle.

Even though Anderson originally introduced it in the form of a tight-binding model with discrete spatial sites, our presented model also exhibits the same behaviour and thus has been used in this report.

2.3 Robustness

We now consider the question of how robust the phenomenon of dynamical localisation is to noise in the kicking potential. For the Anderson model, the localisation is destroyed mainly if there are long-range correlations in the scattering peaks. But we know that the mapping between the Anderson model and the kicked rotor is a nonlinear mapping and hence, it may show a very different behaviour to noise in the kicks.

We investigate the robustness of the kicked rotor model by introducing noise in two different ways:

1. Through kick strengths k: At each time step we add a small noise term to the kick strength k. So $F(k + \delta k)\,|\psi((N-1)\tau)\rangle = |\psi(N\tau)\rangle$.

2. Through kicking periods τ: At each timestep the kick is delivered at time $t = N\tau + \delta\tau$.

This was implemented numerically in the same way as quantum kicked rotor, the only difference being that a new floquet matrix must be generated at each timestep. In the implementation, there is only one point of note - the perturbation in the kicking period must be compensated for on the next step in order to keep the kicking times of the form $t = N\tau + \delta\tau$.

The results are shown in Figure 2.2. The base case shows saturation in the average sq. momentum and highly linear plots for the log of the momentum distribution - both characteristic of localisation. However, the

localisation gets destroyed on adding noise to the kicking strength. The effect is relatively weak in the sense that the noise is nearly 10% of the base kicking strength when we start seeing the localisation completely disappear. At 2% of the base kicking strength, we only see the diffusive behaviour in the variance of sq momentum and weakly in the average sq. momentum, the momentum distribution remains largely localised even after a 1000 timesteps. At 0.1% of the base kicking strength, no effects are visible. This indicates that the system is slightly robust to perturbation in the kicking strength. However, the system shows high sensitivity to perturbations in the time period of the kicking field. Even at noise of scale of 1% of τ, the localisation completely breaks down and diffusive behavour is observed. This shows that the localisation relies on a delicate destructive interference.

2.4 Anderson Transition

The Anderson transition is a second order phase transition occuring in the tight-binding Anderson model of dimension $d > 2$ [5]. The system shows metallic conduction i.e. delocalised states for small values of disorder strength and insulator-like behaviour - localisation for larger values of disorder strength. This phenomenon can be investigated analytically through the use of a scaling function β which describes the behaviour of the (dimensionless) conduction as the length L of the sample changes. This is described in many places such as [5]. We shall not be pursuing that line of attack here.

We have already show the relation between the kicked rotor systems and the Anderson tight-binding models in previous sections. Now we consider a particular case of this. We consider the quasiperiodic kicked rotor:

$$H = \frac{p^2}{2} + \mathcal{K}(t)cos(\theta)\sum_n \delta(t - n\tau) \tag{2.8}$$

where $\mathcal{K}(t) = 1 + \epsilon cos(\omega_2 t + \phi_2)cos(\omega_3 t + \phi_3)$. The dynamics of this 1d system is identical to the following 3d kicked rotor system:

$$H_{3d} = \frac{p_1^2}{2} + p_2\omega_2 + p_3\omega_3 \tag{2.9}$$

$$+ kcos(\theta_1)(1 + \epsilon cos(\theta_2)cos(\theta_3))\sum_n \delta(t - n\tau) \tag{2.10}$$

$$\text{with } |\psi_{3d}(0)\rangle = |\psi_{1d}(0)\rangle\,|\theta_2 = \phi_2\rangle\,|\theta_3 = \phi_3\rangle \tag{2.11}$$

If we consider the fourier transform of the eigenvalue equation for the floquet operator of this Hamiltonian i.e. $F_{3d}\,|\phi_\omega\rangle = e^{i\omega}\,|\phi_\omega\rangle$. Taking a fourier transform of this equation we obtain:

$$\epsilon_{\mathbf{m}}\Phi_{\mathbf{m}} + \sum_{\mathbf{r}\neq 0} W_{\mathbf{r}}\Phi_{\mathbf{m}-\mathbf{r}} = -W_0\Phi_{\mathbf{m}} \tag{2.12}$$

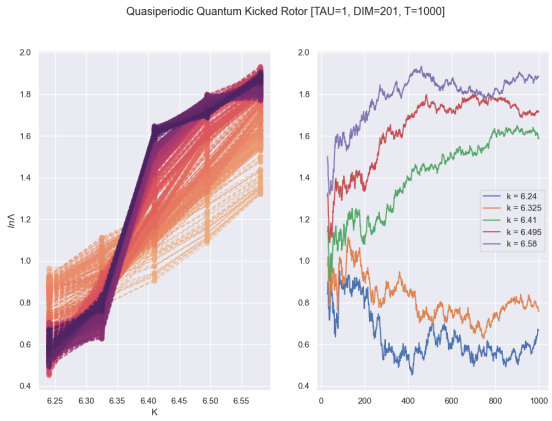

Figure 2.3: The left plot shows the variation of the scaling parameter Λ with k. Each of the lines represents one timestep, darker purple lines are from later timesteps while orange ones are earlier. The point of intersection is the critical point. The transition is known to occur at $k_c = 6.36$ [3]. The right plot shows how Λ changes with time for different values of k sampled.

where $\mathbf{m} = (m_1, m_2, m_3)$ and $\mathbf{r}$ label sites on a 3d lattice and the $\Phi_{\mathbf{m}}$ are related to the fourier components of the floquet eigenstate $|\phi_\omega\rangle$ [2][3].

The quasiperiodic kicked rotor is therefore expected to show a phase transition from delocalised to localised states as the the parameters are varied and certain conditions are satisfied. In particular, the quadruplet $(\hbar, \omega_2, \omega_3, 2\pi)$ should be an incommensurate quadruplet ($\hbar$ is the effective Planck's constant given by $[\theta, p] = i\hbar$). The transition is observed as we increase K and ϵ. In particular, we use a set of values $\hbar = 2.85$, $\omega_2 = 2\pi\sqrt{5}$, $\omega_3 = 2\pi\sqrt{13}$, $K = 6.24 \to 6.58$ and $\epsilon = 0.413 \to 0.462$. [3]

This phase transition has been studied in detail and the author sought to reproduce the results from [3]. [3] uses single parameter scaling theory to utilise simulation data to evaluate properties of the critical point of the transition in order to mitigate finite time effects. The quantity $\Lambda = \langle(p/\hbar)^2\rangle t^{-2/3}$ is the relevant scaling parameter for this transition. The average in $\langle(p/\hbar)^2\rangle$ is an average over initial conditions i.e. over (ϕ_1, ϕ_2).

We could not however, reproduce the scale of the computation done in the paper as it requires computational resources not available to us (40,000 timesteps are a tad bit out of our reach we must say). Nevertheless, we have presented the results from this computation done to best of our resources in Figure 2.3.

2.5 Bipartite Entanglement

The 1d quasiperiodic kicked rotor shows the dynamics of the 3d kicked rotor for a particular value of (ϕ_2, ϕ_3). It doesn't emulate the full rotor as it lacks the degrees

of freedom. Particularly missing from the 1d case is the entanglement between the 1st momentum space and the 2nd, 3rd (quasi)momentum spaces. That the floquet operator entangles the spaces is evident from the calculation of the floquet operator:

$$F_{3d} \tag{2.13}$$

$$= e^{-iKcos\theta_1(1+\alpha cos\theta_2 cos\theta_3)/\hbar} e^{-i(p_1^2/2+p_2\omega_2+p_3\omega_3)/\hbar} \tag{2.14}$$

$$\langle \mathbf{m}| F_{3d} |\mathbf{n}\rangle \tag{2.15}$$

$$= \langle m_1, m_2, m_3| F_{3d} |n_1, n_2, n_3\rangle \tag{2.16}$$

$$= \langle \mathbf{m}| e^{-iKcos\theta_1(1+\alpha cos\theta_2 cos\theta_3)/\hbar} |\mathbf{n}\rangle \tag{2.17}$$

$$e^{-i(\hbar n_1^2/2+n_2\omega_2+n_3\omega_3)} \tag{2.18}$$

$$= \langle \mathbf{m}| \int_{[0,2\pi]^3} d^3\theta \; e^{-iKcos\theta_1(1+\alpha cos\theta_2 cos\theta_3)/\hbar} |\boldsymbol{\theta}\rangle \tag{2.19}$$

$$\langle \boldsymbol{\theta}|\mathbf{n}\rangle \, e^{-i(\hbar n_1^2/2+n_2\omega_2+n_3\omega_3)} \tag{2.20}$$

$$= \int_{[0,2\pi]^3} d^3\theta \;\; \langle \mathbf{m}|\boldsymbol{\theta}\rangle \, e^{-iKcos\theta_1(1+\alpha cos\theta_2 cos\theta_3)/\hbar} \tag{2.21}$$

$$\langle \boldsymbol{\theta}|\mathbf{n}\rangle \, e^{-i(\hbar n_1^2/2+n_2\omega_2+n_3\omega_3)} \tag{2.22}$$

$$= e^{-i(\hbar n_1^2/2+n_2\omega_2+n_3\omega_3)} \frac{1}{(2\pi)^3} \tag{2.23}$$

$$\int_{[0,2\pi]^3} d^3\theta \; e^{-i(\mathbf{m}-\mathbf{n})\cdot\boldsymbol{\theta}} e^{-iKcos\theta_1(1+\alpha cos\theta_2 cos\theta_3)/\hbar} \tag{2.24}$$

$$\approx e^{-i(\hbar n_1^2/2+n_2\omega_2+n_3\omega_3)} DFT_N(f(\boldsymbol{\theta}))[\mathbf{m}-\mathbf{n}] \tag{2.25}$$

where

$$f(\boldsymbol{\theta}) = e^{-iKcos\theta_1(1+\alpha cos\theta_2 cos\theta_3)/\hbar} \tag{2.26}$$

The fourier transform integral clearly mixes up the θ_1, θ_2 and θ_3 terms and hence leads to entanglement. Therefore, we should be able to measure the entanglement between the subspaces $\mathcal{H}_1$ and $\mathcal{H}_{2,3}$. And this is what we attempted to accomplish.

However, several issues arose in doing this. The first and foremost issue was that we need to simulate a 3d quantum system in order to calculate the bipartite entanglement entropy between $\mathcal{H}_1$ and $\mathcal{H}_{2,3}$. Therefore, the memory required and the computational complexity for computing the floquet and density matrices scales as N^6 where N is the size of the momentum eigenbasis being used. The scale of the matrix also requires that the the calculations be done with "double" precision, otherwise it yields underflow errors as some of the fourier transform values are extremely low off the diagonal. Since our basis states are very limited, the approximation of the floquet operator is not very good. A significant portion of calculated eigenvalues of the matrix have absolute values less than even 0.9. This varies for different parameter values but is highest for the higher k values. The calculations are also quite slow to process, however, this was tackled by using C-extensions and parallelisation via Intel OpenMP. As a result, our calculations are not reliable, and therefore, we do not present our numerical analysis here.

2.6 Spectral Analysis

The theory of random matrices has been studied extensively by other people. In this section, we draw from this and try to understand the spectral structure of the floquet matrix. As the floquet operator elements consist of the fourier transform of a kicking function with a pseudo-random strength (at least for longer time scales). So we expect that the elements are randomly distributed. Consequently, we would like to analyse it as a random matrix.

Now random matrix theory makes predictions about the eigenvalue spectrum of the any matrix whose elements are sampled from a gaussian distribution. Depending on the symmetries of the matrix, we can divide it into 3 different ensembles: GUE (Gaussian Unitary Ensemble), GOE (Gaussian Orthogonal Ensemble) and GSE (Gaussian Symplectic Ensemble).

To get an easily observable quantity, we consider the level spacings in the spectrum of these matrices. These theories were made from the viewpoint of analysing the Hamiltonian matrix of different quantum systems. Therefore, the analysed quantity consists of the difference of consecutive eigenvalues i.e. $d_i = \lambda_{i+1} - \lambda_i$. Since the Hamiltonian is hermitian, the λ_i's are real and thus we can talk about consecutive eigenvalues. We define $P(s)$ as the probability distribution of the $s_i = d_i/\bar{d}$ where $\bar{d}$ is the mean level spacing. For systems where the local density of states varies a lot, an 'unfolding' procedure may be required to obtain this. We will not need it and hence, do not describe it.

It can be shown that if the classical analogue of the system is integrable, then the eigenvalues of the matrix are uncorrelated and thus the spacings form a Poisson distribution [6][4]. The systems which have a chaotic classical analogue will fall into one of the 3 mentioned ensembles: GOE (if the system has time inversion invariance and and rotational invariance), GSE (if the system is time inversion invariant but not rotationally invariant) and GUE (in all other cases). A complicated but exact distribution function can be obtained for the level spacings of all of these [4], but Wigner derived a simple formula from the 2×2 matrix case which holds reasonably well, especially for large N. These are listed below [6]:

$$P_{int}(s) = exp(-s) \tag{2.27}$$

$$P_{GOE}(s) = \frac{\pi}{2} s \; exp\left(-\frac{\pi}{4}s^2\right) \tag{2.28}$$

$$P_{GUE}(s) = \frac{32}{\pi^2} s^2 \; exp\left(-\frac{4}{\pi}s^2\right) \tag{2.29}$$

$$P_{GSE}(s) = \frac{2^{18}}{3^6\pi^3} s^4 \; exp\left(-\frac{64}{9\pi}s^2\right) \tag{2.30}$$

However, our kicked rotor systems have time dependent Hamiltonians, and therefore we cannot apply this analysis to it. However, it turns out that we can use the same strategy on the eigenenergies. These are the phase angles of the eigenvalues of the floquet matrix. It turns out that their distribution is nearly identical to the guassian ensembles' eigenvalues. Therefore, there exist analogues of each of the ensembles called COE (Circular Orthogonal Ensemble), CUE (Circular Unitary Ensemble) and CSE (Circular Symplectic Ensemble). Since the space of these phases is compact $[0, 2\pi)$, we also avoid complications with unfolding as the density of states is uniform $\frac{N}{2\pi}$ (N being the number of eigenphases). Correspondingly, we define

$$s = \frac{2\pi}{N}(\phi_{i+1} - \phi_i) \tag{2.31}$$

where ϕ_i are the eigenphases of the floquet operator arranged in increasing order. We can also define the consecutive level spacing ratio distribution $P(r)$ where r is defined as:

$$r_i = \frac{s_{i+1}}{s_i} \tag{2.32}$$

Now using the same techniques as used in deriving the Wigner surmises, good approximations can be found for the ratio distributions from the 3×3 matrix case. The ratio distribution also doesn't require unfolding of any kind. The surmises takes the form[1]:

$$P_W(r) = \frac{1}{Z_\beta} \frac{(r + r^2)^\beta}{(1 + r + r^2)^{1+3\beta/2}} \tag{2.33}$$

where β is the Dyson index which is 1 for COE, 2 for CUE and 4 for CSE. The Z_β are normalisation constants which can be found in [1].

For the purposes of this project, attempts were made to calculate the level spacing ratio distributions for the quasiperiodic kicked rotor systems. However, the same problems as the last section still plague us as the approximating floquet matrix has a maximum of 21 basis states in each of the three directions owing to computational resource limitations. Therefore, those results are not presented here.

Chapter 3

Epilogue

3.1 Future Prospects

1. The calculations for metal-insulator transition properties in the quasiperiodic kicked rotor can be enhanced through C-extensions and parallelisation as done for the 3d quasiperiodic kicked rotor.

2. The calculations for the bipartite entanglement entropy can be repeated on a workstation with better computational resources and the same holds for the spectral analysis.

3. One can try and investigate kicked rotor systems with perturbative driving such as $H = p^2/2 + kcos(\theta)\sum_n \delta(t-n) + \lambda Acos(l\theta)$ where $A << V$. Such a small driving term may be useful in using the system as a quantum computer if it conserves the localisation. If we take a small value of l, we may be able to use the adiabatic theorem to change the phase of system to attain some optimal configuration over several iterations (such as in Grover's algorithm) while maintaining localisation.

3.2 Conclusion

We have discussed in some detail an overview of the phenomena that occur in the quantum kicked rotor system and its variants. We have presented numerical analysis of the kicked rotor and its robustness to noise in the kicking strength and the time period of kicking. We have also presented relevant background for the calculation of the bipartite entanglement entropy between the first and the remaining momentum spaces and for the spectral analysis of the floquet matrices of the kicked rotor systems.

Bibliography

[1] Y. Y. Atas et al. "The distribution of the ratio of consecutive level spacings in random matrix ensembles". In: *Phys. Rev. Lett.* 110.8 (Feb. 21, 2013), p. 084101. ISSN: 0031-9007, 1079-7114. DOI: 10.1103/PhysRevLett.110.084101. arXiv: 1212.5611. URL: http://arxiv.org/abs/1212.5611 (visited on 05/14/2021).

[2] Shmuel Fishman, D R Grempel, and R E Prange. "Chaos, Quantum Recurrences, and Anderson Localization". In: 49.8 (1982), p. 4.

[3] G. Lemarié, B. Grémaud, and D. Delande. "Universality of the Anderson transition with the quasiperiodic kicked rotor". In: *Europhys. Lett.* 87.3 (Aug. 1, 2009), p. 37007. ISSN: 0295-5075, 1286-4854. DOI: 10.1209/0295-5075/87/37007. URL: https://iopscience.iop.org/article/10.1209/0295-5075/87/37007 (visited on 04/21/2021).

[4] M. L. Mehta. *Random matrices*. Amsterdam: Elsevier, 2004. ISBN: 1280968184 9781280968181 9786610968183 6610968187.

[5] Cord A. Müller and Dominique Delande. "Disorder and interference: localization phenomena". In: *arXiv:1005.0915 [cond-mat, physics:quant-ph]* (June 1, 2016). arXiv: 1005.0915. URL: http://arxiv.org/abs/1005.0915 (visited on 04/21/2021).

[6] Hans-Jürgen Stöckmann. *Quantum Chaos: An Introduction*. Cambridge University Press, 1999.